# An Atmospheric Dry Intrusion Parameter and Its Application*

WANG Donghai[1†](王东海) and YANG Shuai[2](杨 帅)

1 *State Key Laboratory of Severe Weather (LaSW), Chinese Academy of Meteorological Sciences, Beijing* 100081

2 *Laboratory of Cloud-Precipitation Physics and Severe Storms (LACS), Institute of Atmospheric Physics, Chinese Academy of Sciences, Beijing* 100029

(Received February 24, 2010)

**ABSTRACT**

Dry intrusion plays an important role in the explosive development of cyclones and the evolution of cold fronts. Characteristics of dry intrusion during a rainfall event that occurred in northern China are analyzed in detail in this paper. The IM (ingredients-based methodology) developed by Doswell et al. in 1996 and Wetzel and Martin in 2001 is utilized. All the physical representations of dry intrusion defined in the past studies, such as low relative humidity, cold advection, and high potential vorticity (on either isobaric or isentropic surfaces), are combined into a simple and convenient physical parameter to characterize dry intrusion. This is a new attempt to extend the IM that was primarily applied to research on heavy rainfall to the study of dry intrusion. The new dry intrusion parameter is used to analyze the isentropic evolution of dry intrusion during the rainfall event. The results show that this parameter can better quantify the intensity of dry intrusion and diagnose its evolution shown in satellite infrared and water vapor imageries. It is found that dry intrusion maintains during the rainfall period. The intensity of precipitation increases with the increasing dry intrusion, which has pushed the rainy region southeastward. From the results on the isentropic surface and the corresponding isobaric surface, it is inferred that the analyses of dry intrusion on both surfaces are consistent with each other. The isentropic analysis of dry intrusion reveals that cold and dry air at the upper level overruns that in the lower troposphere where moist and warm air is located. Thus, potential instability is built up in the vertical direction, which favors the occurrence of precipitation. In practice, we may identify dry intrusion regions by tracking strong signals of the dry intrusion parameter, and further identify the instability near the dry intrusion regions. This will aid in improving the accuracy of precipitation forecast.

**Key words:** dry intrusion, parameter, isentropic analysis

**Citation:** Wang Donghai and Yang Shuai, 2010: An atmospheric dry intrusion parameter and its application. *Acta Meteor. Sinica*, **24**(4), 492–500.

## 1. Introduction

Dry intrusion occurs when cold and dry air with high values of potential vorticity (PV) intrudes from the lower stratosphere and/or upper troposphere down towards the lower troposphere. Danielsen (1964) demonstrated the three-dimensional structure of a dry intrusion airflow fanning out from tropopause and then folding down into a surface cold front along an isentropic surface. Dry intrusion is referred to as "dry slots" in satellite infrared images and "dark areas" in water vapor images (Browning and Monk, 1982; Browning et al., 1995).

Browning and Monk (1982) provided a split cold front model, with an upper-level front overlaying a surface front. In this model, the cold and dry airflows behind the upper-level cold front exerted significant impacts on the frontal precipitation. Browning and Roberts (1994) used numerical weather prediction (NWP) model products together with satellite and radar images and put forward a conceptual model of a developing midlatitude frontal cyclone, elucidating the influence of dry intrusion on the evolution of the rapidly deepening cyclone. Browning and Golding (1995) used radar and satellite imageries and a mesoscale NWP model to analyze a rapidly deepening cyclone that moved across the British Isles. The air mass in the form of a mesoscale dry intrusion

*Supported by the National Natural Science Foundation of China under Grant Nos. 40633016 and 40805001, and the Open Project of the State Key Laboratory of Severe Weather, Chinese Academy of Meteorological Sciences, under Grant No. 2009LASW-B02.

†Corresponding author: wangdh@cams.cma.gov.cn.

(Chinese version published in Vol. 67, No. 4, 522–529, 2009)

descended from the near-tropopause level, which appeared to overrun parts of the warm conveyor belt ahead of a surface cold front and induced potential instability, and then triggered frontal convective precipitation. Browning et al. (1995) studied the effect of dry intrusion on mesoscale structure and evolution of a frontal cyclone over the eastern North Atlantic. Browning and Roberts (1996) illuminated the effect of dry intrusion on precipitation triggered by cold fronts. They traced the origin of dry intrusion–the airflows with high PV intruding from near the tropopause folding. In detail, they also diagnosed how the circulation composed of lower-level warm conveyor belt and upper-level dry intrusion triggered active convective precipitation. Browning (1997) analyzed the development of extra-tropical cyclones affected by dry intrusion, and pointed out that the cyclone deepening phase is associated with both the ascending motion of moist air and the dry intrusion airflow from the upper troposphere above the cyclone center. He derived a conceptual model of inter-twisting between dry intrusion and moist upward airflows near the cyclone center. Spencer and Stensrud (1998) studied the role of dry cold air on the development of heavy precipitation by numerical simulations. They showed that, using the convective parameterization scheme including the lagged-downdraft airflow, precipitation is better simulated by taking account of the effect of dry cold air. Yu and Yao (2003) made a review on the dry intrusion and its application. Yao and Yu (2005) studied the activity of dry cold air and its impacts on Meiyu rainfall during the 2003 Meiyu period. Yao et al. (2007) analyzed the dry intrusion process associated with a low vortex along the Meiyu front.

In summary, dry intrusion has played an important role in the explosive deepening of cyclones (Wakimoto et al., 1992), the evolution of cold fronts, the associated frontal precipitation, etc. It can often be seen from synoptic charts that dry intrusion descends and reaches a level above a warm and moist sector, which may induce potential instability, allowing further strong convection with precipitation to be triggered by some perturbation. Therefore, research on characteristics of dry intrusion is very important for weather analysis and forecasting.

On the basis of the work by McNulty (1978, 1995), some researchers (Doswell, 1987; Johns and Doswell, 1992; and Doswell et al., 1996) developed the ingredients-based methodology Wetzel and Martin (2001) applied the IM to the routine analysis and forecast of midlatitude winter precipitation. They included several physical variables, such as ascending motion, moisture, instability, temperature, etc., into the IM. They also provided a new parameter: potential vorticity and divergence of the Q-vector (PVQ), which combined the two ingredients (the forced ascending and the instability index) of the IM to predict the duration, intensity, and type of winter precipitation. Can the IM that was used mainly for precipitation analysis be adopted in the study of dry intrusion? In the previous studies, a single physical variable such as low relative humidity, or cold advection, or high PV, etc., is applied to dry intrusion analysis on isobaric or isentropic surfaces. Can these single variables be integrated into a simple and convenient physical parameter to represent dry intrusion? This is a new attempt to extend the IM from the research of heavy rainfall to dry intrusion. A new dry intrusion parameter is configured and applied to the analysis of the evolution of a dry intrusion process.

## 2. Dry intrusion parameter

Many previous studies about dry intrusion are made on isentropic surface (e.g., Browning et al., 1995) because isentropic analysis provides convenience to trace the origin, track, and three-dimensional structure of dry intrusion. Since dry intrusion involves the cold dry air with high PV from the tropopause, a new parameter can be defined to quantify the dry intrusion and its evolution.

This new dry intrusion parameter is defined as:

$$P_\theta = \frac{(-\boldsymbol{V} \cdot \nabla_\theta \Phi)\, V_{\mathrm{P}\theta}}{Tf}, \tag{1}$$

where the subscript "$\theta$" denotes "isentropic", and variables $\boldsymbol{V}$, $\Phi$, $V_{\mathrm{P}}$, $T$, and $f$ represent horizontal velocity (m s$^{-1}$), geopotential height (gpm), potential vorticity (PVU), absolute temperature (K), and relative humidity (%) on the isentropic surface, respectively.

The new parameter has clear physical meanings. Firstly, regarding the denominator, a small $T$ value denotes cold air and a small $f$ value represents dry air. Secondly, as for the numerator, a large $V_{\mathrm{P}}$ value denotes air with high potential vorticity and $-\boldsymbol{V}\cdot\nabla_\theta\Phi$ shows the origin of cold dry airflow: when $-\boldsymbol{V}\cdot\nabla_\theta\Phi > 0$, the air descends from upper level to lower level. With the integrated consideration of $\boldsymbol{V}$, $\Phi$, $V_{\mathrm{P}}$, $T$, $f$, etc., the strong dry intrusion is identified by a large value of positive $P_\theta$.

To testify the validity of this dry intrusion parameter on isentropic surface, two equivalents are provided on isobaric surface and under Cartesian coordinate system as shown below:

$$P_p = \frac{(-\boldsymbol{V}\cdot\nabla_p T)V_{\mathrm{P}p}}{Tf}, \tag{2}$$

$$P_z = \frac{(-\boldsymbol{V}\cdot\nabla_z T)V_{\mathrm{P}z}}{Tf}. \tag{3}$$

## 3. A case study

### *3.1 Synoptic background and precipitation characteristics*

The case with dry intrusion in northern China from 0000 UTC 12 to 0000 UTC 13 August 2004 is analyzed as an example. Figure 1 shows the observed 24-h cumulative precipitation from 0000 UTC 12 to 0000 UTC 13 August 2004. Three precipitation maxima along a southwest-northeast rainband in northern China can be seen at (37°N, 113°E), (37.5°N, 114.5°E), and (39°N, 117.5°E), respectively. On the synoptic scale, a strong confluence belt and a typical "saddle" pattern exist on the northwest-west edge of the subtropical high (Fig. 2a); a deep trough with a northeast-southwest orientation stretches from (46°N, 126°E) to (40°N, 110°E) at 700 hPa. At 200 hPa, the study area is dominated by a divergent flow induced by the South Asian high (Fig. 2b). Therefore, the lower-level confluence is overlapped with the upper-level divergence. This case is simulated using the three-dimensional nonhydrostatic weather research and forecasting (WRF) model. Detailed analyses on the numerical schemes and the comparison between the observations and the WRF model simulated results of this case can be found in Yang et al. (2007). In the present study, reliable outputs from the model are used to diagnose the dry intrusion process.

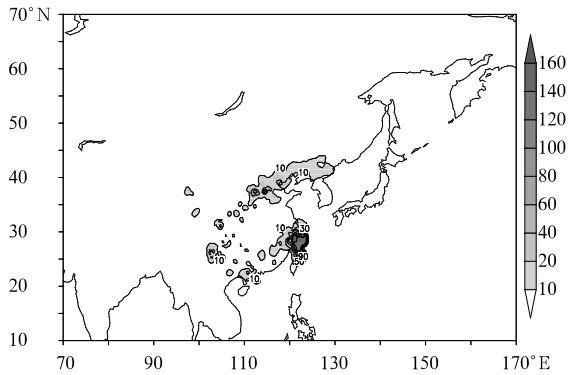


**Fig. 1.** The observed 24-h accumulated precipitation (mm) from 0000 UTC 12 to 0000 UTC 13 August 2004.

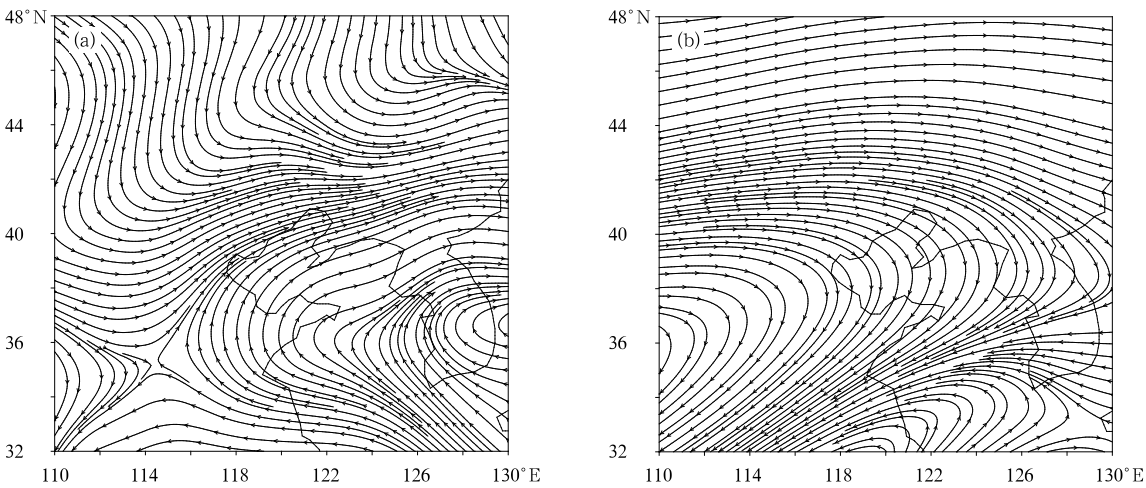


**Fig. 2.** Streamline fields at (a) 700 hPa and (b) 200 hPa at 0000 UTC 12 August 2004.

### *3.2 The dry intrusion analysis*

Because it is convenient to use isentropic analysis to trace the origin, track, and three-dimensional structure of dry intrusion, $P_\theta$ in Eq. (1) is calculated on isentropic surface using the WRF model results in order to obtain characteristic distributions of dry intrusion for the rainfall case. The distributions are then validated by utilizing satellite water vapor and infrared imageries. As a contrast to isentropic analyses, $P_p$ in Eq. (2) on isobaric surface is also calculated in the meantime.

From the satellite water vapor and infrared imageries (Fig. 3) and the 6-h cumulative precipitation distributions (Fig. 4), it is seen that rainfall occurred below the cloud belt between 105° and 140°E, and south of 50°N (Figs. 3b and 3d). In the satellite water vapor imagery (Figs. 3a and 3c), a bright belt appeared with evident dry regions to both its north and south. Figure 5a shows that the large-value centers of positive $P_\theta$ located at (47°N, 120°E), (54°N, 137°E), and (36°N, 135°E) corresponded with the three "dark areas" in the satellite water vapor imagery (Fig. 3a), the cloud-free areas in the infrared imagery (Fig. 3b), and the dry regions (with low relative humidity) where winds from upper levels (about 9000 m) traversing isolines of geopotential height descended to lower levels (about 4000 m) (Fig. 5b). Precipitation just occurred below the cloud belt, south of the positive $P_\theta$ (Figs. 3b and 4a). From Fig. 5a, it is seen that the dry intrusion (with strong positive $P_\theta$) was located near 45° and at about 500 hPa. The distribution of $P_p$ at 500 hPa is given in Fig. 5c, in which the areas of strong positive $P_p$ nearly matched the dry areas and dry advection on the 320-K isentropic surface, especially near 45° and 36°N. Two $P_p$ centers between 45° and 50°N and another center near 36°N (Fig. 5c) corresponded with the $P_\theta$ centers north of 45°N and near 36°N in Fig. 5a, and were situated in the dry regions in Fig. 5d. It can be inferred that the features of dry intrusion on both surfaces (isentropic surface and corresponding isobaric surface) are consistent. Distributions of $P_\theta$ and $P_p$ on 320-K isentropic surface and at 500-hPa level can indicate the strong dry intrusion in this case.

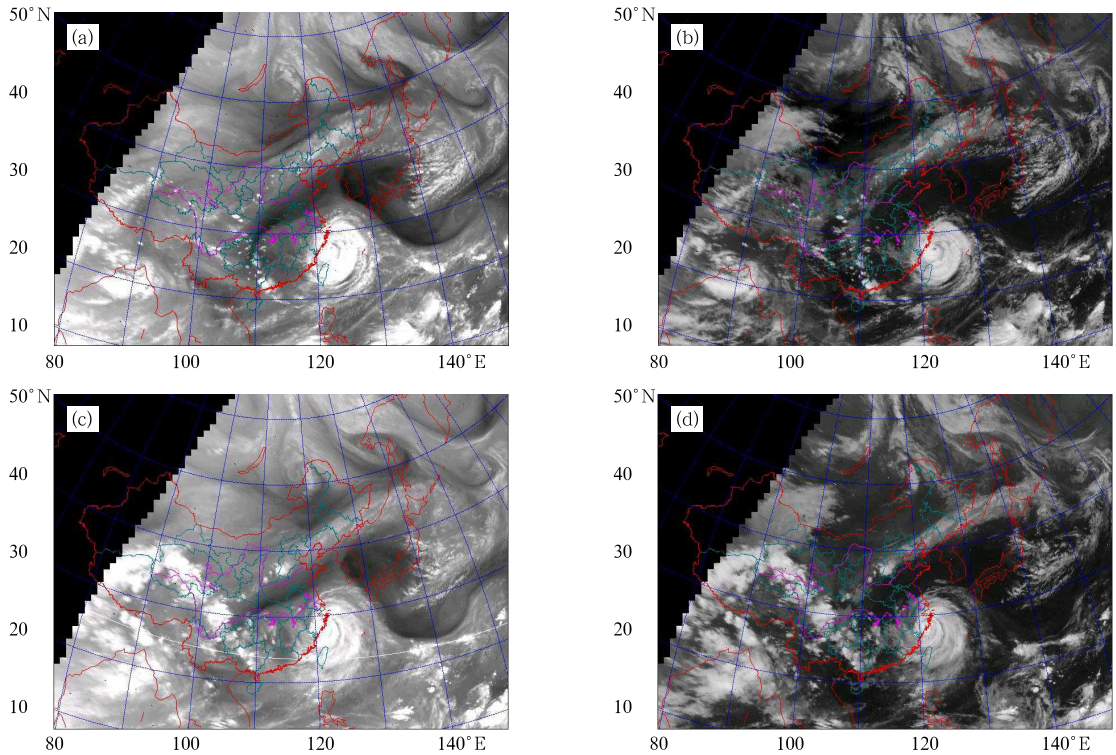


**Fig. 3.** The FY-2C satellite water vapor imagery at (a) 0600 UTC and (c) 1200 UTC, and the FY-2C infrared imagery at (b) 0600 UTC and (d) 1200 UTC 12 August 2004.

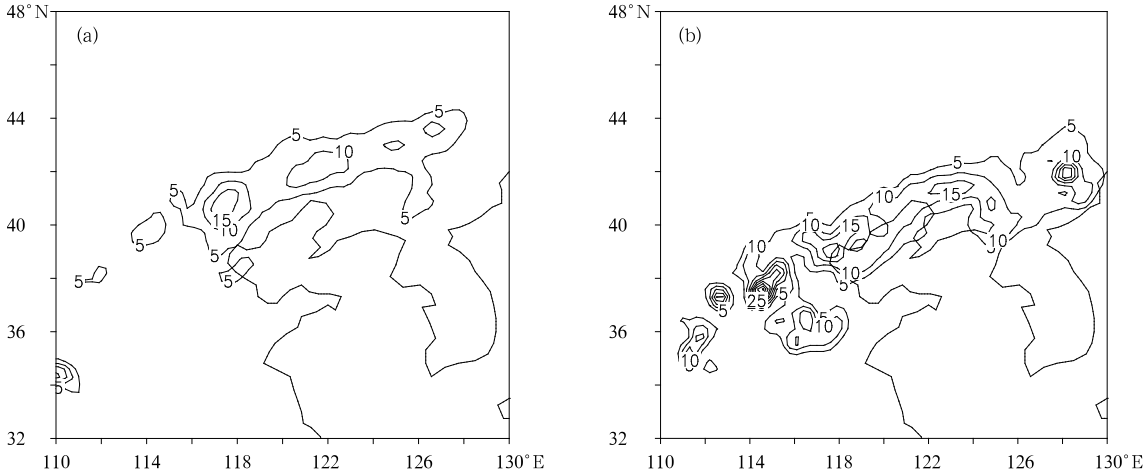


**Fig. 4.** The observed 6-h accumulated precipitation (mm) over North China from (a) 0000 to 0600 UTC and (b) 0600 to 1200 UTC 12 August 2004.

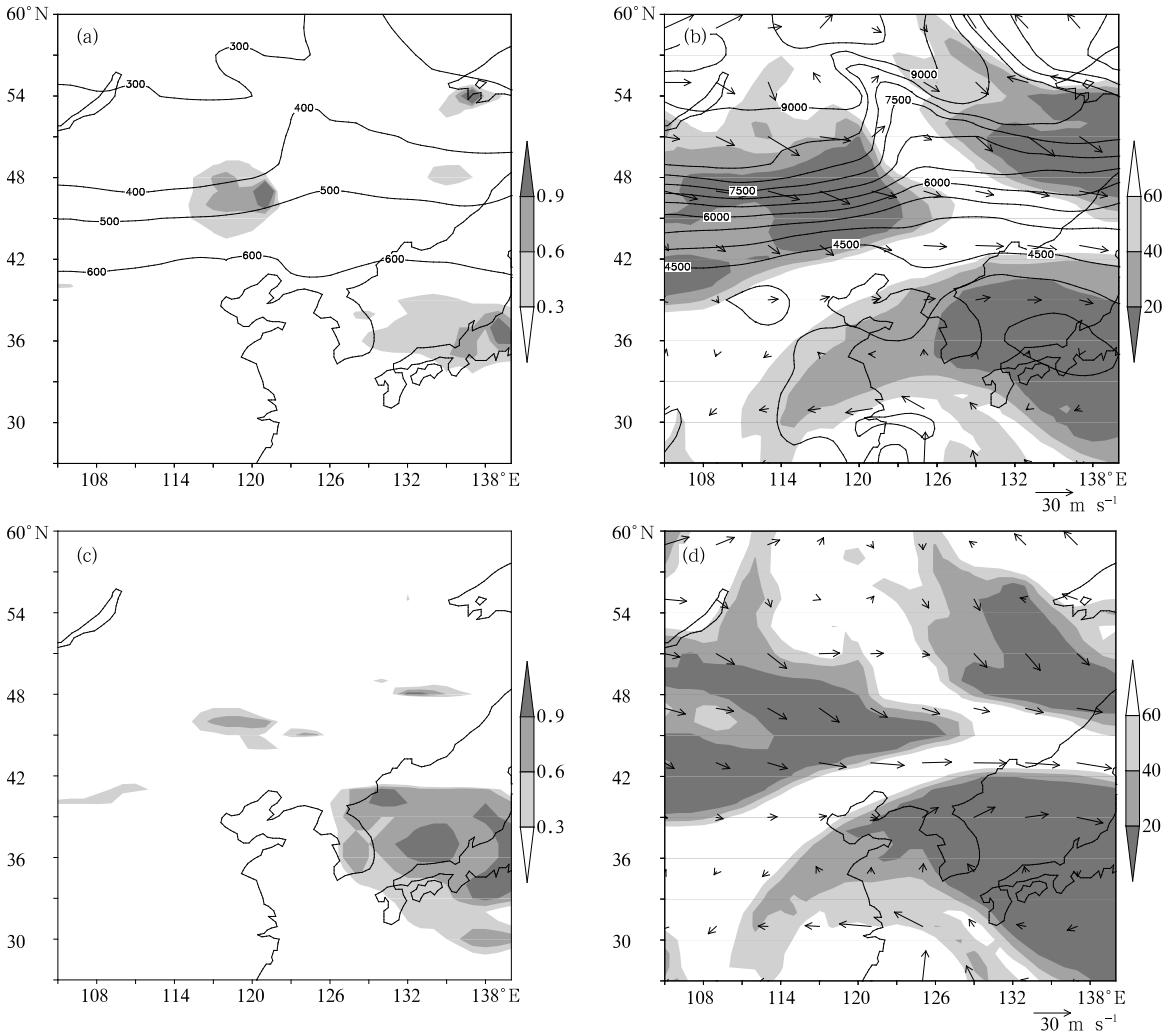


**Fig. 5.** (a) $P_\theta$ (shaded; $10^{-7}$ m$^4$ s$^{-4}$ kg$^{-1}$) and pressure (isolines; hPa) on 320-K isentropic surface; (b) horizontal wind vector (arrows; m s$^{-1}$), geopotential height (isolines; gpm), and relative humidity (shaded; %) on 320-K isentropic surface; (c) $P_{\rm p}$ (shaded; $10^{-11}$ m$^2$ K s$^{-2}$ kg$^{-1}$) at 500 hPa; (d) horizontal wind vector (arrows; m s$^{-1}$), and relative humidity (shaded; %) at 500 hPa at 0600 UTC 12 August 2004.

At 1200 UTC 12 August 2004, the positive $P_\theta$ and $P_p$ moved southward (Figs. 6a and 6c), and the dark areas in the satellite water vapor imagery (Fig. 3c) and the dry areas in Figs. 6b and 6d moved southward correspondingly. The values of both $P_\theta$ and $P_p$ increased. In Fig. 4, rain belts also moved southward, and the 6-h cumulative precipitation amount had an increase as well. This suggests that the arrival of dry intrusion pushed the rain belts southeastward.

Figures 7a and 7b depict distributions of temperature advection and PV on 320-K isentropic surface. The strong dry intrusion (positive-value centers in Figs. 5a and 5c) was dominated by strong cold advection (indicated by the strong negative temperature advection in Fig. 7a). Figure 7b displays that the PV = 1 isoline extends downward to 4500–5000 m. Some PV centers, such as the two located at (52°N, 115°E) and (51°N, 140°E) in Fig. 7b, are distributed within the dry regions (Figs. 5b and 5d). It is shown that the strong dry intrusion from mid and upper tropospheres (with large $P_\theta$ and $P_p$) was caused by the coactions among the high-PV air intruding from the upper levels, the large downward winds traversing geopotential height isolines, the cold temperature advection, and low temperature as well as low humidity.

The variables such as $P_\theta$, relative humidity, horizontal wind, and geopotential height on 342- and 310-K isentropic surfaces at 0600 and 1200 UTC 12 August 2004 are also analyzed (figure omitted). Similar to those on 320-K isentropic surface, positive

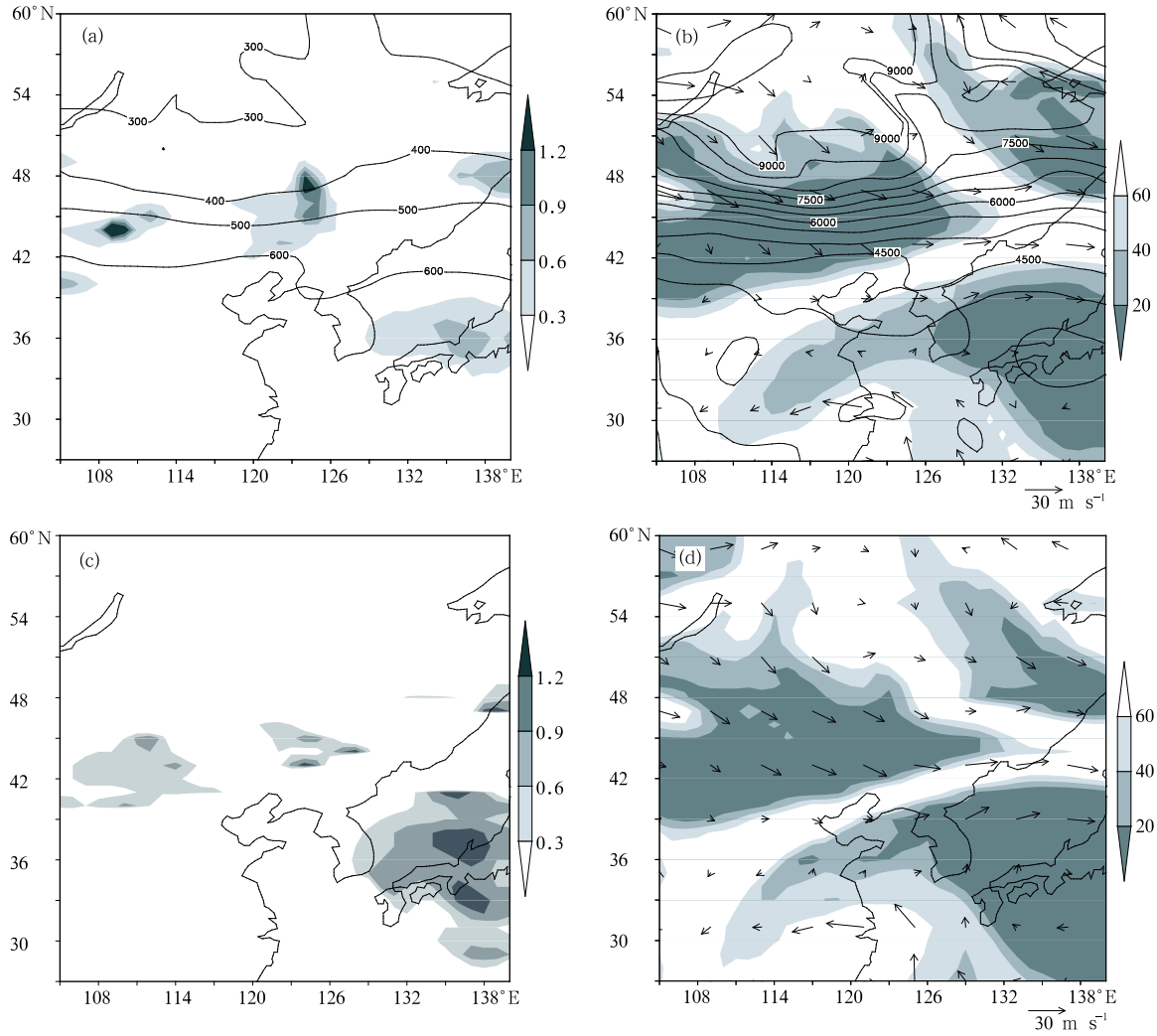


**Fig. 6.** As in Fig. 5, but at 1200 UTC 12 August 2004.

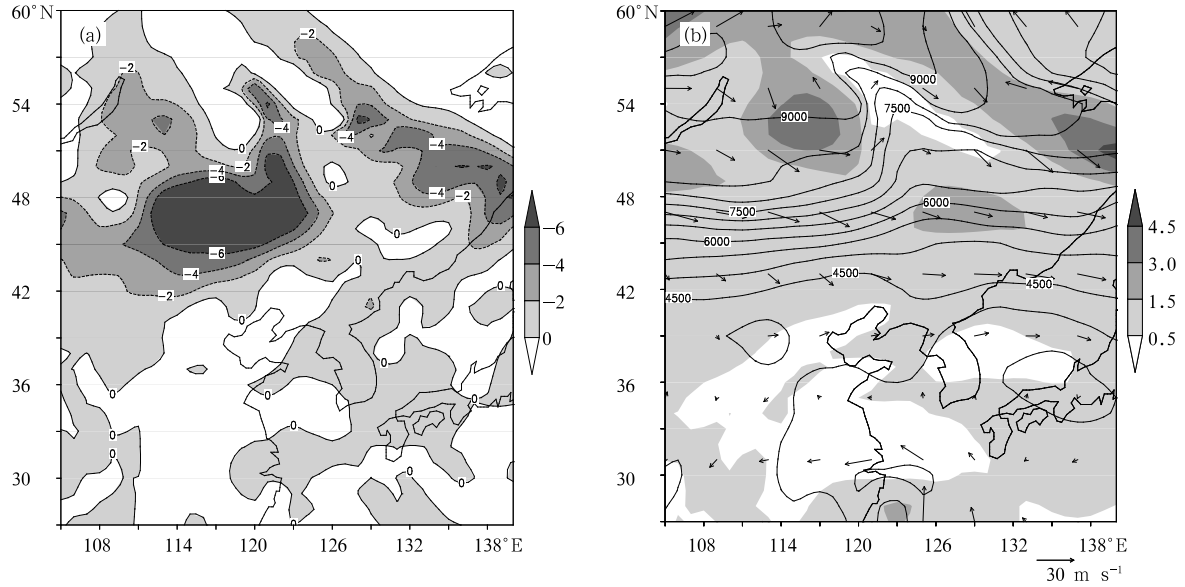


**Fig. 7.** (a) Horizontal temperature advection ($10^{-4}$ K s$^{-1}$); (b) isentropic potential vorticity (shaded; PVU), geopotential height (isolines; gpm), and horizontal wind (vectors; m s$^{-1}$) on 320-K isentropic surface at 0600 UTC 12 August 2004.

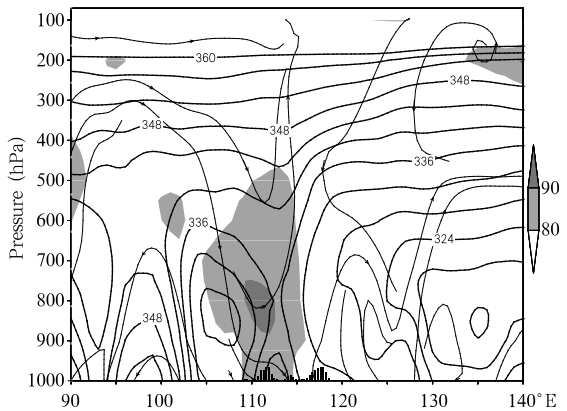


**Fig. 8.** The zonal-vertical cross-section along 38°N of equivalent potential temperature (isolines; K), streamline field, and relative humidity (shaded; %) at 0600 UTC 12 August 2004. The histogram of simulated 6-h accumulated precipitation (mm) from 0000 UTC to 0600 UTC 12 August 2004 is shown at the bottom.

$P_\theta$ corresponded to the dry airflows from the upper level (about 11 km) descending towards the lower level (about 8.5 km), while the negative $P_\theta$ accompanying the positive $P_\theta$ was located in warm moist ascending airflows. It is also found that the strong dry intrusion (with strong $P_\theta$ signals) in the north of 40°N on 342-K isentropic surface was located at about 300 hPa. Therefore, the distributions of $P_p$, relative humidity, and wind vectors at 300 hPa were analyzed. The results show that the dry intrusion features on 342- and 310-K isentropic surfaces are basically consistent with those at 300 and 700 hPa.

If the dry air intruding from upper levels with relative humidity equal to 20% is defined as a critical dry intrusion, the critical values of $P_\theta$ and $P_p$, denoted as $(P_\theta)_{\rm cr}$ and $(P_p)_{\rm cr}$, respectively, are calculated and listed in Table 1. For the rainfall case, the coverage of strong dry intrusion is better indicated by regions with $P_\theta$ and $P_p$ larger than $(P_\theta)_{\rm cr}$ and $(P_p)_{\rm cr}$. It is found that precipitation occurred at the leading side of the motion of strong dry intrusion, i.e., southeast of the strong dry intrusion. The strong dry intrusion also pushed precipitation to move southeastward.

In addition, another case from 0000 UTC 23 to

**Table 1.** Dry intrusion parameters for the August 2004 case

| Isobaric surface (hPa) | $(P_p)_{\rm cr}$ ($10^{-11}$ m$^2$ K s$^{-2}$ kg$^{-1}$) | Isentropic surface (K) | $(P_\theta)_{\rm cr}$ ($10^{-7}$ m$^4$ s$^{-4}$ kg$^{-1}$) |
|---|---|---|---|
| 300 | 1.0 | 342 | 0.6 |
| 500 | 0.3 | 320 | 0.3 |
| 700 | 0.1 | 310 | 0.06 |

0000 UTC 24 July 2005 is also studied. The same conclusion is obtained. Because the critical value of strong dry intrusion is obtained from only two cases in this paper, the results derived hereby are considered preliminary. The critical values need to be validated by more cases.

By comparison of the dry intrusion parameters on 342-, 320-, and 310-K isentropic surfaces, it is found that both $P_\theta$ and $P_p$ increase with height, indicating that the dry intrusion is stronger at upper levels than at lower levels and is originated from the higher levels. The zonal-vertical cross-section along 38°N of the equivalent potential temperature, streamline, relative humidity, and cumulative precipitation (Fig. 8) shows that cold dry westerlies from upper levels evidently intruded downward till 850 hPa, reached above the warm and moist sector, then moved eastward, and ascended between 110° and 115°E. The precipitation near 112°E was controlled by the ascending airflow. Near 120°E, another cold and dry upper-level westerly airflow descended to about 500 hPa, and reached above the rainy regions near 117°E.

The above analyses reveal that the parameter we defined can synthetically characterize dry intrusion in the manifestation of low temperature, low humidity, high potential vorticity, etc., and can trace the origin and track of cold air as well. Therefore, this is a suitable parameter to describe dry intrusion.

## 4. Summary

The characteristics of dry intrusion during a rainfall event that occurred in northern China are examined and analyzed in detail in this study. A new dry intrusion parameter is used to delineate the isentropic evolution, to trace the origin and track, and to study the three-dimensional structure of the dry intrusion. The results show that this new parameter performs better in quantifying the intensity of dry intrusion and diagnosing the evolution of dry intrusion from satellite and water vapor imageries. It is found that the analyses of dry intrusion on both isentropic surface and corresponding isobaric surface are equivalently useful. Furthermore, precipitation got enhanced with stronger dry intrusion, and dry intrusion might have pushed the rainy region to migrate southeastward during this rainfall event.

The isentropic analysis of dry intrusion during the August 2004 rainfall event discloses that dry intrusion was present at several height levels, but its intensity was larger in the upper troposphere (see Table 1). The upper-level cold and dry air overran that in the lower troposphere, and was situated right above the low-level moist and warm atmosphere (Fig. 8). Thus, potential instability was built up following the increasing gradients of temperature and humidity in the vertical, which favored the occurrence of precipitation. This hints that we could firstly identify dry intrusion regions by tracing strong signals of the dry intrusion parameter, and then the instability near the dry intrusion regions can be found, which is helpful for the precipitation forecast. This method may thus aid in improving the accuracy and efficiency of precipitation forecast. In future work, we may derive the tendency equations of the dry intrusion parameter based on Eqs. (1), (2), and (3) and predict the dry intrusion development. This is one more potential application of the dry intrusion parameter.

## REFERENCES

Browning, K. A., 1997: The dry intrusion perspective of extra-tropical cyclone development. *Meteor. Appl.*, **4**, 317–324.

——, and G. A. Monk, 1982: A simple model for the synoptic analysis of cold fronts. *Quart. J. Roy. Meteor. Soc.*, **108**, 435–452.

——, and N. M. Roberts, 1994: Structure of a frontal cyclone. *Quart. J. Roy. Meteor. Soc.*, **120**, 1535–1557.

——, and B. W. Golding, 1995: Mesoscale ascepts of a dry intrusion within a vigorous cyclone. *Quart. J. Roy. Meteor. Soc.*, **121**, 463–493.

——, S. A. Clough, C. S. Davitt, et al., 1995: Observations of the mesoscale sub-structure in the clod air of a developing frontal cyclone. *Quart. J. Roy. Meteor. Soc.*, **121**, 1229–1254.

——, and N. M. Roberts, 1996: Variation of frontal and precipitation structure along a cold front. *Quart. J. Roy. Meteor. Soc.*, **122**, 1845–1872.

Danielsen, E. F., 1964: Project Springfield Report. Defense Atomic Support Agency, Washington D. C.,

20301, DASA 1517 (NTIS AD-607980), 99 pp.

Doswell, C. A., 1987: The distinction between large-scale and mesoscale contribution to severe convection: A case study example. *Wea. Forecasting*, **2**, 3–16.

——, H. E. Brooks, and R. A. Maddox, 1996: Flash flood forecasting: An ingredients-based methodology. *Wea. Forecasting*, **11**, 560–581.

Johns, R. H., and C. A. Doswell, 1992: Severe local storms forecasting. *Wea. Forecasting*, **7**, 588–612.

McNulty, R. P., 1978: On upper tropospheric kinematics and severe weather occurrence. *Mon. Wea. Rev.*, **106**, 662–672.

——, 1995: Severe and convective weather: A central region forecasting challenge. *Mon. Wea. Rev.*, **10**, 187–202.

Spencer, P. L., and D. J. Stensrud, 1998: Simulating flash flood events: importance of the subgrid representation of convection. *Mon. Wea. Rev.*, **126**(11), 2884–2192.

Wakimono, R. M., W. Blier, and C. Liu, 1992: The frontal structure of an explosive oceanic cyclone: Airborne radar observations of ERICA IOP 4. *Mon. Wea. Rev.*, **120**(7), 1135–1155.

Wetzel, S. W., and J. E. Martin, 2001: An operational ingredients-based methodology for forecasting mid-latitude winter season precipitation. *Wea. Forecasting*, **16** (1), 156–167.

Yang Shuai, Gao Shouting, and Wang Donghai, 2007: A study of Richardson number and instability in moist saturated flow. *Chinese J. Geophy.*, **50**(2), 365–375. (in Chinese)

Yao Xiuping and Yu Yubin, 2005: Activity of dry cold air and its impacts on Meiyu rain during 2003 Meiyu period. *Chinese J. Atmos. Sci.*, **29**, 973–985. (in Chinese)

——, Wu Guoxiong, Zhao Bingke, et al., 2007: The studies of dry intrusion associated with vortex precipitation along Meiyu front. *Science in China (Ser. D)*, **37**, 417–428. (in Chinese)

Yu Yubin and Yao Xiuping, 2003: Reviews on the dry intrusion and its application. *Acta Meteor. Sinica*, **61**, 669–778. (in Chinese)